tually perpendicular.[1] In $[Cu(2,5\text{-DTH})Cl_2]$ and $[Cu(4,7\text{-DTD})Cl_2]$, the Cu_2Cl_2 plane essentially bisects the angle formed by the two Cu_2S_2 planes. It has been observed that the relative orientation of the exchange-coupled entities in chains influences the magnitude of the exchange coupling constant,[20] and this work shows that this feature is particularly important in determining the magnitude of J in these alternating-chain compounds.

As noted above, there are two short interchain contacts which could lead to superexchange pathways and magnetic interactions. The S(2)···S(1) interchain distance of 3.857 Å would provide the superexchange pathway Cu–S···S–Cu, but this may reasonably be expected to be less important than the shorter Cu–S···Cu pathway. There is also a short S(2)···Cu interchain distance of 4.943 Å, and these contacts, when taken in pairs, appear to link dimers into spin ladders. However, exchange by a single interchain Cu···S–Cu pathway should be less important than exchange through two Cu···S–Cu pathways, and in view of the alternating-chain magnetism, the latter must predominate.

Exchange coupling may be transmitted through long nonbonded contacts involving sulfur atoms. The sulfur–sulfur contact between molecular units in $[(C_2H_5)_4N][Ni(DDDT)_2]$ (DDDT is 5,6-dihydro-1,4-dithiin-2,3-dithiolate) is 3.98 Å, yet these are exchange-coupled into two-dimensional layers with $J = -8.5$ cm^{-1}, and even though the nickel–nickel interlayer separation is 8.152 Å, $[(C_2H_5)_4N][Ni(DDDT)_2]$ undergoes long-range order near 15 K.[21] EPR evidence and molecular orbital calculations show that there is substantial delocalization of electron density onto the ligand in $[(C_2H_5)_4N][Ni(DDDT)_2]$, and this permits the intermolecular exchange interaction.

The structure and properties of the mixed-valence compound $Cu^I_2Cu^{II}(2,5\text{-DTH})_6(ClO_4)_4$ are germane to this discussion.[22,23] Copper ions in $[Cu(2,5\text{-DTH})_2]^{q+}$ ($q = 1$ or 2) complexes have tetrahedral coordination, and there is no distinction between copper(I) and copper(II). That is, the copper(I) and copper(II) ions are randomly distributed in the cations in the solid state. The mechanism responsible for making all copper ions equivalent, even though they are separated by 8 Å, is probably mediated by long nonbonded sulfur–sulfur interactions that facilitate rapid electron transfer.

Long, nonbonded sulfur–copper contacts of 3.98 Å in $[Cu(4\text{-METZ})(DMF)Cl_2]_2$ gave rise to ladderlike magnetism, and a relatively large mean-field J' of -1.0 cm^{-1} has been found for $[Cu(C_4H_5NS)_2Cl_2\cdot CH_3OH]_2$.[24] These intermolecular interactions may be understood in terms of superexchange pathways involving long nonbonded contacts between dimeric units. The large radial extensions of the sulfur orbitals permit these unexpectedly large interdimer exchange interactions.

Acknowledgment. This work was supported by the National Science Foundation by Grant No. CHE 83 08129. We thank Richard M. Kessler and Jeffrey S. Beller for experimental assistance.

Registry No. $[Cu(2,5\text{-DTH})Cl_2]_2$, 99727-67-0; $[Cu(4,7\text{-DTD})Cl_2]_2$, 99727-68-1; 4,7-DTD, 22037-97-4; $CH_3CH_2CH_2SH$, 107-03-9; $ClCH_2CH_2Cl$, 107-06-2.

Supplementary Material Available: Tables of anisotropic thermal parameters, hydrogen atom coordinates, and structure factor amplitudes (18 pages). Ordering information is given on any current masthead page.

(21) Vance, C. T.; Bereman, R. D.; Bordner, J.; Hatfield, W. E.; Helms, J. H. *Inorg. Chem.* **1985**, *24*, 2905.

(22) Musker, W. K.; Olmstead, M. M.; Kessler, R. M.; Murphey, M. B.; Neagley, C. H.; Roush, P. B.; Hill, N. L.; Wolford, T. L.; Hope, H.; Delker, G.; Swanson, K.; Gorewit, B. V. *J. Am. Chem. Soc.* **1980**, *102*, 1225.

(23) Olmstead, M. M.; Musker, W. K.; Kessler, R. M. *Inorg. Chem.* **1981**, *20*, 151.

(24) Marsh, W. E.; Helms, J. H.; Hatfield, W. E.; Hodgson, D. J., submitted for publication.

Contribution from the Department of Chemistry, McMaster University, Hamilton, Ontario L8S 4M1, Canada

The $XeN(SO_2F)_2^+$ and $F[XeN(SO_2F)_2]_2^+$ Cations: Syntheses, Raman and Multinuclear Magnetic Resonance Studies of the AsF_6^- and $Sb_3F_{16}^-$ Compounds, and X-ray Structure of $XeN(SO_2F)_2^+Sb_3F_{16}^-$

Romolo Faggiani, Dietmar K. Kennepohl, Colin J. L. Lock, and Gary J. Schrobilgen*

Received December 28, 1984

Like its XeF_2 precursor, the Xe–N-bonded $FXeN(SO_2F)_2$ molecule exhibits fluoride ion donor properties that, in the present work, have resulted in the syntheses of adducts having the stoichiometries $FXeN(SO_2F)_2\cdot AsF_5$, $FXeN(SO_2F)_2\cdot 3SbF_5$, and $2FXeN(SO_2F)_2\cdot AsF_5$. All compounds have been enriched to 30% with ^{15}N and studied by ^{15}N, ^{19}F, and ^{129}Xe NMR spectroscopy and Raman spectroscopy. The spectroscopic studies have shown the above stoichiometries to be consistent with the predominantly ionic formulations $XeN(SO_2F)_2^+AsF_6^-$, $XeN(SO_2F)_2^+Sb_3F_{16}^-$, and $F[XeN(SO_2F)_2]_2^+AsF_6^-$. In general, the cations are thermally less stable than their fluorine analogues, XeF^+ and $Xe_2F_3^+$. The crystal structure of $XeN(SO_2F)_2^+Sb_3F_{16}^-$ has been obtained at −64 °C from three-dimensional X-ray data. [Bis(fluorosulfuryl)amido]xenon(II) hexadecafluorotriantimonate(V) crystallizes in the monoclinic system, space group $P2_1/c$, with four molecules in a unit cell of dimensions $a = 10.320$ (2) Å, $b = 10.642$ (2) Å, $c = 18.167$ (3) Å, and $\beta = 108.94$ (1)°. The structure was solved by the heavy-atom method and refined by least-squares and Fourier methods to a final R factor of 0.061 for 2376 observed ($F > 0$) reflections. The structure analysis has established the existence of discrete $XeN(SO_2F)_2^+Sb_3F_{16}^-$ molecules and shows that the $XeN(SO_2F)_2^+$ cation is Xe–N bonded and that the Xe–N bond (2.02 (1) Å) is significantly shorter than in $FXeN(SO_2F)_2$ (2.200 (3) Å). The $Sb_3F_{16}^-$ anion is cis-fluorine bridged and weakly covalently bonded by means of a fluorine bridge to the $XeN(SO_2F)_2^+$ cation (Xe···F = 2.457 (8) Å).

Introduction

Compounds containing xenon–fluorine and xenon–oxygen bonds have been known since the inception of noble-gas chemistry.[1] They include such compounds as XeF_2,[2] XeF_4,[3] XeF_6,[4] $XeOF_4$,[4] XeO_2F_2,[5] $FXeOSO_2F$,[6,7] $FXeOTeF_5$,[8] and $F_3XeOIOF_4$.[9] The first xenon–nitrogen compound to be reported, $FXeN(SO_2F)_2$,

(1) Bartlett, N. *Proc. Chem. Soc., London* **1962**, 218.
(2) Hoppe, R.; Dahne, W.; Mattauch, H.; Rodder, K. M. *Angew. Chem.* **1962**, *74*, 903; *Angew. Chem., Int. Ed. Engl.* **1962**, *1*, 599.
(3) Claassen, H. H.; Selig, H.; Malm, J. G. *J. Am. Chem. Soc.* **1962**, *84*, 3593.
(4) Malm, J. G.; Sheft, I.; Chernick, C. L. *J. Am. Chem. Soc.* **1963**, *85*, 110.
(5) Houston, J. L. *J. Phys. Chem.* **1967**, *71*, 3339.
(6) Wechsburg, M.; Bulliner, P. A.; Sladky, F. O.; Mews, R.; Bartlett, N. *Inorg. Chem.* **1972**, *11*, 3063.
(7) Gillespie, R. J.; Schrobilgen, G. J. *Inorg. Chem.* **1974**, *13*, 1694.
(8) Sladky, F. *Monatsh. Chem.* **1970**, *101*, 1559, 1571, 1578.

0020-1669/86/1325-0563$01.50/0

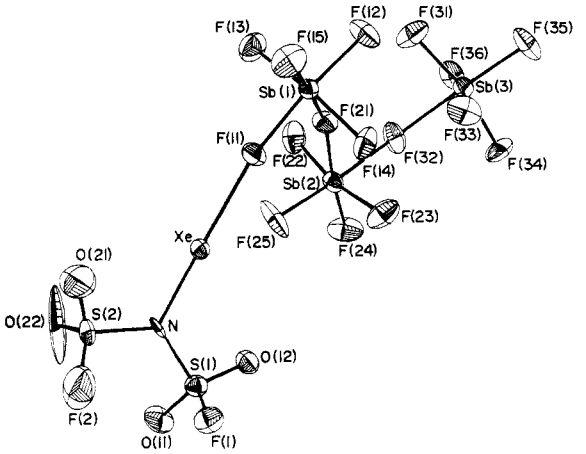

Figure 1. Perspective drawing of the $XeN(SO_2F)_2^+Sb_3F_{16}^-$ structural unit showing the numbering scheme and some bond lengths (Å) (thermal ellipsoids are drawn at the 50% probability level).

was prepared by DesMarteau and LeBlond[10] in 1974 and has only recently been definitively characterized, confirming the existence of the first xenon–nitrogen bond, with use of X-ray crystallography, multinuclear magnetic resonance spectroscopy, and Raman spectroscopy by Schrobilgen et al.[11] Recently, $Xe[N(SO_2F)_2]_2$ was prepared,[12] and later the ^{15}N-enriched compound was also synthesized and definitively characterized with use of multinuclear magnetic resonance spectroscopy and Raman spectroscopy.[13] The bis compound $Xe[N(SO_2F)_2]_2$, a white solid, liquifies and simultaneously decomposes rapidly when warmed to near room temperature.

Although the use of the $N(SO_2F)_2$ group to stabilize xenon in its +2 oxidation state has been clearly established, neither $FXeN(SO_2F)_2$ nor $Xe[N(SO_2F)_2]_2$ are as thermally stable as xenon(II) compounds having ligating oxygen or fluorine atoms. More recently, $Xe[N(SO_2CF_3)_2]_2$ has been prepared and has been partially characterized with use of mass spectrometry, Raman spectroscopy, and ^{19}F and ^{129}Xe NMR spectroscopy.[14,15] The white solid compound $Xe[N(SO_2CF_3)_2]_2$, in contrast to $Xe[N(SO_2F)_2]_2$, is thermally stable at room temperature, and significant decomposition only occurs upon warming to 72 °C.

In addition to a class of neutral Xe(II) compounds, several examples of Xe(II) cations also exist. These cations include XeF^+,[16] $Xe_2F_3^+$,[17-19] and $(XeF)_2SFO_3^+$[6,7] (V-shaped SO_3F-bridged species), all with their appropriate counterions, such as AsF_6^-, SbF_6^-, and $Sb_2F_{11}^-$. The first xenon–nitrogen adduct reported possessed the stoichiometry $2FXeN(SO_2F)_2 \cdot AsF_5$ and was postulated to have the ionic formulation $F[XeN(SO_2F)_2]_2^+AsF_6^-$.[12] This xenon–nitrogen cation was prepared according to eq 1 and 2.[13] Solution studies by ^{19}F and ^{129}Xe NMR spectroscopy in BrF_5

$$FXeN(SO_2F)_2 + AsF_5 \xrightarrow{-78\ °C} XeN(SO_2F)_2^+AsF_6^- \quad (1)$$

$$2XeN(SO_2F)_2^+AsF_6^- \xrightarrow[\text{vacuum}]{23\ °C} F[XeN(SO_2F)_2]_2^+AsF_6^- + AsF_5 \quad (2)$$

Table I. Selected Interatomic Distances (Å) and Angles (deg)

		Distances	
Xe–N	2.02 (1)	Sb(1)–F(11)	1.903 (8)
Xe---F(11)	2.457 (8)	Sb(1)–F(12)	1.833 (9)
Xe---F(33)[a]	3.063 (9)	Sb(1)–F(13)	1.842 (8)
Xe---F(25)	3.10 (1)	Sb(1)–F(14)	1.837 (8)
Xe---F(34)[a]	3.15 (1)	Sb(1)–F(15)	1.83 (1)
Xe---F(14)[a]	3.168 (8)	Sb(1)–F(21)	2.062 (9)
Xe---F(36)[a]	3.200 (9)		
N–S(1)	1.70 (1)	Sb(2)–F(21)	2.022 (9)
N–S(2)	1.68 (1)	Sb(2)–F(22)	1.811 (9)
		Sb(2)–F(23)	1.835 (8)
S(1)—O(11)	1.39 (1)	Sb(2)–F(24)	1.85 (1)
S(1)–O(12)	1.40 (1)	Sb(2)–F(25)	1.85 (1)
S(1)–F(1)	1.518 (9)	Sb(2)–F(32)	1.955 (9)
S(2)–O(21)[b]	1.37 (1)	Sb(3)–F(32)	2.092 (8)
S(2)–O(22)[b]	1.34 (1)	Sb(3)–F(31)	1.84 (1)
S(2)–F(2)[b]	1.40 (2)	Sb(3)–F(33)	1.86 (1)
		Sb(3)–F(34)	1.842 (9)
		Sb(3)–F(35)	1.843 (9)
		Sb(3)–F(36)	1.857 (9)
		Angles	
N–Xe–F(11)	178.3 (3)	F(13)–Sb(1)–F(11)	88.0 (4)
N–Xe–F(14)[a]	106.4 (3)	F(13)–Sb(1)–F(12)	91.6 (4)
N–Xe–F(34)[a]	112.2 (4)	Sb(1)–F(21)–Sb(2)	154.7 (5)
N–Xe–F(25)	116.1 (4)	F(21)–Sb(2)–F(22)	84.9 (4)
N–Xe–F(33)[a]	71.3 (4)	F(21)–Sb(2)–F(23)	84.3 (4)
N–Xe–F(36)[a]	64.5 (4)	F(21)–Sb(2)–F(24)	174.5 (4)
Xe–N–S(1)	118.1 (6)	F(21)–Sb(2)–F(25)	87.4 (4)
Xe–N–S(2)	117.9 (6)	F(21)–Sb(2)–F(32)	84.4 (4)
S(1)–N–S(2)	123.6 (7)	F(24)–Sb(2)–F(22)	94.1 (4)
N–S(1)–O(11)	107.7 (6)	F(24)–Sb(2)–F(23)	95.9 (4)
N–S(1)–O(12)	105.5 (6)	F(24)–Sb(2)–F(25)	98.1 (5)
N–S(1)–F(1)	99.5 (6)	F(24)–Sb(2)–F(32)	90.1 (4)
N–S(2)–O(21)[b]	103.5 (8)	F(23)–Sb(2)–F(25)	92.2 (4)
N–S(2)–O(22)[b]	107.6 (7)	F(23)–Sb(2)–F(32)	85.0 (4)
N–S(2)–F(2)[b]	105.3 (8)	F(22)–Sb(2)–F(25)	95.6 (4)
O(11)—S(1)–O(12)	125.5 (7)	F(22)–Sb(2)–F(32)	85.7 (4)
O(11)–S(1)–F(1)	107.8 (6)	F(25)–Sb(2)–F(32)	171.6 (4)
F(1)–S(1)–O(12)	107.8 (5)	Sb(2)–F(32)–Sb(3)	153.7 (5)
O(21)–S(2)–O(22)[b]	113 (1)	F(32)–Sb(3)–F(31)	83.2 (4)
O(21)–S(2)–F(2)[b]	109 (1)	F(32)–Sb(3)–F(33)	84.0 (4)
F(2)–S(2)–O(22)[b]	117 (1)	F(32)–Sb(3)–F(34)	83.4 (4)
Xe–F(11)–Sb(1)	169.6 (4)	F(32)–Sb(3)–F(35)	178.1 (4)
F(15)–Sb(1)–F(11)	93.3 (4)	F(32)–Sb(3)–F(36)	84.9 (4)
F(15)–Sb(1)–F(12)	98.6 (4)	F(35)–Sb(3)–F(31)	98.6 (4)
F(15)–Sb(1)–F(13)	95.8 (4)	F(35)–Sb(3)–F(33)	95.2 (4)
F(15)–Sb(1)–F(14)	95.6 (4)	F(35)–Sb(3)–F(34)	94.8 (4)
F(21)–Sb(1)–F(11)	83.0 (4)	F(35)–Sb(3)–F(36)	95.8 (4)
F(21)–Sb(1)–F(12)	85.0 (4)	F(33)–Sb(3)–F(31)	89.0 (5)
F(21)–Sb(1)–F(13)	84.5 (4)	F(33)–Sb(3)–F(34)	89.2 (4)
F(21)–Sb(1)–F(14)	83.9 (4)	F(36)–Sb(3)–F(31)	90.4 (4)
F(21)–Sb(1)–F(15)	176.4 (4)	F(36)–Sb(3)–F(34)	88.7 (4)
F(14)–Sb(1)–F(11)	86.6 (4)		
F(14)–Sb(1)–F(12)	91.5 (4)		

[a] Intermolecular distances or angles. [b] Distances may be artifically short because of disorder in the $S(2)O_2F$ group. Similarly, angles involving S(2) as the central atom may be distorted because of disorder.

and SO_2ClF solvent media have also been reported for this cation.[13] Like its $Xe_2F_3^+$[17-19] and $Kr_2F_3^+$[20] analogues, the $F[XeN(SO_2F)_2]_2^+$ cation is postulated to be fluorine bridged. However, solution studies of $F[XeN(SO_2F)_2]_2^+$, unlike those of $Xe_2F_3^+$ and $Kr_2F_3^+$, have failed to produce evidence for nonlabile (on the NMR time scale) Xe---F---Xe bridges. This has been attributed to the dissociative equilibria represented by eq 3 and 4.[13]

$$F[XeN(SO_2F)_2]_2^+ \rightleftarrows FXeN(SO_2F)_2 + XeN(SO_2F)_2^+ \quad (3)$$

$$F[XeN(SO_2F)_2]_2^+ \rightleftarrows Xe[N(SO_2F)_2]_2 + XeF^+ \quad (4)$$

To date, there has been only one X-ray structure determination of a xenon–nitrogen compound, namely $FXeN(SO_2F)_2$,[11] and there

(9) Schrobilgen, G. J.; Syvret, R. G. *J. Chem. Soc., Chem. Commun.* **1985**, 1529.
(10) LeBlond, R. D.; DesMarteau, D. D. *J. Chem. Soc., Chem. Commun.* **1974**, 555.
(11) Sawyer, J. F.; Schrobilgen, G. J.; Sutherland, S. J. *Inorg. Chem.* **1982**, *21*, 4064.
(12) DesMarteau, D.; LeBlond, D.; Hassain, S. F.; Nöthe, D. *J. Am. Chem. Soc.* **1981**, *103*, 7734.
(13) Schumacher, G. A.; Schrobilgen, G. J. *Inorg. Chem.* **1983**, *22*, 2178.
(14) Foropoulos, J., Jr.; DesMarteau, D. D. *J. Am. Chem. Soc.* **1982**, *104*, 4260.
(15) Schrobilgen, G. J., unpublished work.
(16) Burgess, J.; Fraser, C. J. W.; McRae, V. M.; Peacock, R. D.; Russell, D. R. *Inorg. Nucl. Chem., Suppl.* **1976**, 183.
(17) Gillespie, R. J.; Landa, B. *Inorg. Chem.* **1973**, *12*, 1383.
(18) Gillespie, R. J.; Netzer, A.; Schrobilgen, G. J. *Inorg. Chem.* **1974**, *13*, 1455.
(19) Bartlett, N.; DeBoer, B. G.; Hollander, F. J.; Sladky, F. O.; Templeton, D. H.; Zalkin, A. *Inorg. Chem.* **1974**, *13*, 780.
(20) Gillespie, R. J.; Schrobilgen, G. J. *Inorg. Chem.* **1976**, *15*, 22.

are no examples of xenon–nitrogen cations that have been definitively characterized. The present work is concerned with the syntheses and first complete characterization of novel examples of xenon–nitrogen cations using X-ray crystallography, multinuclear magnetic resonance spectroscopy, and Raman spectroscopy.

Results and Discussion

Crystal Structure of $XeN(SO_2F)_2^+Sb_3F_{16}^-$. The structural analysis shows that crystals of $XeN(SO_2F)_2^+Sb_3F_{16}^-$ consist of an ordered assembly of discrete fluorine-bridged cations and anions (Figure 1 and Figure 2 (supplementary material)) in which the xenon atom is bonded to the nitrogen atom of the $N(SO_2F)_2$ ligand. Table I gives a selected list of interatomic distances and angles for the $XeN(SO_2F)_2^+Sb_3F_{16}^-$ structural unit.

The $XeN(SO_2F)_2^+$ cation is structurally similar to the neutral compound, $FXeN(SO_2F)_2$, whose crystal structure has been reported recently.[11] The xenon of the $XeN(SO_2F)_2^+$ cation is only weakly covalently bonded to a fluorine. This fluorine is, however, more strongly bonded to the anion, giving rise to a fluorine-bridge interaction between the anion and the cation. Consequently, some important differences can be noted between the $XeN(SO_2F)_2^+$ cation and $FXeN(SO_2F)_2$. The neutral compound has a covalent F–Xe bond distance of 1.967 (3) Å compared to the much longer bridging Xe---F bond distance between the cation and the anion of 2.457 (8) Å. The decrease in bond order of Xe---F in the cation results in an increase in the Xe–N bond order as is evidenced by the shorter Xe–N bond length of 2.02 (1) Å in the cation compared to 2.200 (3) Å in $FXeN(SO_2F)_2$. Similar bond length changes have been reported for the fluorine analogue, XeF_2, which has a Xe–F bond length of 2.010 (6) Å,[21] while the fluorine-bridged XeF^+ cation in $XeF^+Sb_2F_{11}^-$ has a terminal Xe–F bond length of 1.84 (1) Å.[22]

A distorted-tetrahedral arrangement is observed for the oxygens and fluorines bonded to the sulfurs of the SO_2F groups. The large O–S–O bond angles, compared to the expected 109.5° for a regular tetrahedral arrangement, are consistent with bond-pair–bond-pair repulsions between two sulfur–oxygen bonds possessing considerable double-bond character (Table I). As a result, the remaining angles around sulfur deviate from their tetrahedral values, giving average N–S–F, N–S–O, and O–S–F angles of 99.5, 106.6, and 107.8°, respectively. The two SO_2F groups show quite different behavior. One is well located, but the other shows large thermal motion, and this is probably caused by disorder. Bond lengths and bond angles within the group are also consistent with this. Thus in the ordered SO_2F unit the S–F bond is significantly longer than the S–O bonds (1.518 (9) vs. 1.39 (1), 1.40 (1) Å) and the O(11)–S–O(12) angle of 125.5 (7)° is much larger than the tetrahedral angle. In the disordered molecule there is no significant difference in the S–O and S–F bond lengths and the O(21)–S–O(22) angle (113 (1)°) is much smaller than O(11)–S–O(12) and not significantly different from O(21)–S–F(2) or O(22)–S–F(2). At least two positions and probably all three represent occupancy by both fluorine and oxygen atoms. A number of disorder models were tried involving permutation of the fluorine and oxygen atoms and also partial occupancy of atomic positions, but none of these models gave a significant improvement over the model reported here.

The fluorine and oxygen atoms on the SO_2F group are oriented at a torsion angle of approximately 35° to the atoms on the other SO_2F group. The relative orientations adopted by the SO_2F groups serve to minimize intramolecular repulsions among the oxygen and fluorine atoms of the SO_2F groups. The dihedral angle formed by two planes, containing the fluorine and two oxygens, on the SO_2F groups, is about 56°, and the S–N–S bond angle is approximately 124°. The above two planes are perpendicular to the N–S bonds, indicating a minimum contact point in the Xe, N, S(1), S(2) plane (Figure 3 (supplementary material)). It is at this point that maximum repulsion between fluorines and oxygens on sulfur will occur. The minimum possible interatomic distances between the two SO_2F groups have been calculated in the plane by using the known bond angles and lengths and was found to be 2.04 Å for F(1)---O(22), while the actual sum of the van der Waals radii for oxygen and fluorine is 3.0 Å. The SO_2F groups clearly must adopt a semistaggered orientation with fluorine and oxygen atoms avoiding the Xe, N, S(1), S(2) plane (Figure 4 (supplementary material)).

The N–Xe---F arrangement, like N–Xe–F (178.1 (1)°) in $FXeN(SO_2F)_2$, is very nearly linear (178.3 (3)°). This linear arrangement is found in all Xe(II) compounds and is consistent with the VSEPR rules[23] for the AX_2E_3 formulation of the three lone pairs in equatorial positions with the bond pairs in axial positions about the central Xe(II) atom. Significant intra- and intermolecular close contacts around the xenon atom seem to avoid the equatorial region of the N–Xe---F(11) system, presumably due to the lone-pair electron density on xenon. All close contacts, within the sum of their van der Waals radii (Xe---F = 3.63 Å, Xe---O = 3.68 Å), are either less than 71° or greater than 106°, with respect to the N–Xe---F(11) system, and are similar to those in the neutral compound. The close contacts with the terminal fluorines on antimony that are less than 3.50 Å are listed in Table I. The Xe–F(11)–Sb(1) bridge bond angle is 169.6 (4)° and is appreciably larger than in $XeF^+Sb_2F_{11}^-$ (147°).[16] It would seem that this angle is rather easily distorted by packing considerations and that its exact value is perhaps not highly significant.

The Xe, S(1), and S(2) atoms form an essentially trigonal-planar arrangement about nitrogen with a S–N–S bond angle of 123.6 (7)° and Xe–N–S bond angles of 118.1 (6)°. This planar arrangement around nitrogen as well as the relatively short S–N bond (1.70 (1) Å) indicate double-bond character arising from the involvement of the nitrogen lone pair in sulfur–nitrogen $p\pi$–$d\pi$ bonding. The S–N single-bond length is assumed to be the 1.772 Å value found in sulfamic acid, $H_3N^+SO_3^-$, where no electrons are available on nitrogen for π bonding.[24] The S–N bond distance of 1.70 (1) Å in $XeN(SO_2F)_2^+$ is only slightly greater than in other S–N π-bonded systems such as $K[NH_2SO_3]$ (1.666 (6) Å)[25] and $K_2[NH(SO_3)_2]$ (1.674 (5) Å)[26] and is comparable to the S–N distance in $K_3[N(SO_3)_3]\cdot 2H_2O$ (1.71 (2) Å).[27] The N–S bond length in the $XeN(SO_2F)_2^+$ cation is clearly indicative of substantial S–N double-bond character. Both the planar arrangement around nitrogen and an even shorter S–N bond length (1.625 (3) Å)[11] are found in $FXeN(SO_2F)_2$. The resonance hybrid structures I and II represent the principal contributing structures for the $XeN(SO_2F)_2^+$ cation fluorine-bridged to the anion. Thus, the

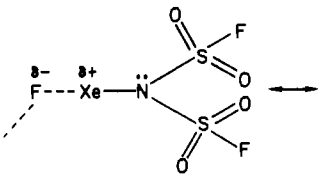

I

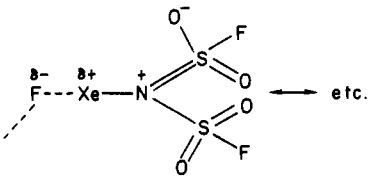

II

S–N bond should be longer in the cation than in neutral $FXeN(SO_2F)_2$ owing to the net positive charge buildup on adjacent xenon and nitrogen atoms in the cation.

(21) Levy, H. A.; Argon, P. A. *J. Am. Chem. Soc.* **1963**, *85*, 241.
(22) Bartlett, N. *Endeavour* **1972**, *31*, 107.
(23) Gillespie, R. J. "Molecular Geometry"; Van Nostrand-Reinhold: London, 1972.
(24) Bats, J. W.; Coppens, P.; Koetzle, T. F. *Acta Crystallogr., Sect. B: Struct. Crystallogr., Cryst. Chem.* **1977**, *B33*, 37.
(25) Jeffrey, G. J.; Stadler, J. *J. Chem. Soc.* **1951**, 1467.
(26) Jeffrey, G. J.; Jones, D. W. *Acta Crystallogr.* **1956**, *9*, 283.
(27) Tillack, J. V.; Kennard, C. H. L. *J. Chem. Soc. A* **1970**, 1637.

Table II. ^{19}F NMR Parameters for the $XeN(SO_2F)_2^+$ Cation and Related Xenon–Nitrogen Compounds

species	$\delta_{^{19}F}$	solvent	temp, °C
$XeN(SO_2F)_2^+$	67.9	SbF_5	25
$[N(SO_2F)_2]_2$	58.7		
F on Sb			
F_1	−86		
F_2	−104		
F_3	−140		
$Xe[N(SO_2F)_2]_2$[b]	60.2	SO_2ClF	−40
$FXeN(SO_2F)_2$[b]	−126.0 (F on Xe)		
$[N(SO_2F)_2]_2$[b]	58.0		

[a] Referenced with respect to neat $CFCl_3$ at 24 °C. [b] Reference 13.

The X-ray crystal structure of the trans-fluorine-bridged $Sb_3F_{16}^-$ anion has been reported for $Br_2^+Sb_3F_{16}^-$ by Edwards et al.[28] The present work describes the first X-ray crystal structure determination for a cis-fluorine-bridged $Sb_3F_{16}^-$ anion. The Sb–F(terminal) distances average 1.84 ± 0.02 Å, and the Sb–F(bridge) distances average 2.01 ± 0.08 Å compared to 1.83 ± 0.07 Å and 2.03 ± 0.07 Å, respectively, in the trans-fluorine-bridged anion. The cis-fluorine-bridged network is distorted with the cis fluorines and antimony atoms subtending angles of 84°; the bridging Sb---F---Sb angles are 154°. Adjacent SbF_6 units in $Sb_3F_{16}^-$ are oriented along the Sb–F–Sb bridge such that the terminal equatorial fluorines on each pair of adjacent SbF_6 units are staggered with respect to one another. There is also an "umbrella" effect, wherein the terminal equatorial fluorines on antimony bend away (96°) from the terminal fluorine trans to the bridging fluorine. The bridging fluorine bonds are weaker than the terminal bonds, resulting in a trans effect and trans terminal Sb–F bonds which are shorter than the other terminal Sb–F bonds. These shorter bonds in turn lead to repulsions of the other terminal Sb–F bond pairs, distorting the regular octahedral arrangement about antimony.

NMR Spectroscopy of the $XeN(SO_2F)_2^+$ Cation. Solutions of $[^{15}N]$-$F[XeN(SO_2F)_2]^+AsF_6^-$ (30% ^{15}N enrichment) in SbF_5 were studied by ^{129}Xe, ^{19}F, and ^{15}N NMR spectroscopy at room temperature. Dissolution of $F[XeN(SO_2F)_2]_2^+AsF_6^-$ in SbF_5 solvent resulted in the displacement of the weaker fluoride ion acceptor, AsF_5, by SbF_5 according to eq 5. Three broad signals were found

$$F[XeN(SO_2F)_2]_2^+AsF_6^- + nSbF_5 \xrightarrow{\text{excess } SbF_5} XeN(SO_2F)_2^+Sb_nF_{5n+1}^- + AsF_5 \quad (5)$$

at −86, −104, and −140 ppm (relative peak areas 1:2:2) in the room-temperature ^{19}F NMR spectrum, in good agreement with the reported values of the fluorine chemical shifts for the three fluorine environments found in polymeric liquid SbF_5.[29] A low-frequency fluorine-on-xenon signal corresponding to $FXeN(SO_2F)_2$ (−126.1 ppm at −58 °C in BrF_5 solvent) is absent in the ^{19}F NMR spectrum of the $XeN(SO_2F)_2^+$ cation. Rather, a sharp high-frequency peak at 67.9 ppm is assigned to the fluorine-on-sulfur environment of the $XeN(SO_2F)_2^+$ cation and a sharp weak peak at 58.7 ppm arising from the room-temperature decomposition product $[N(SO_2F)_2]_2$ was observed (Table II). The bright yellow solutions slowly decomposed at room temperature and have a half-life of ca. 1 day. The decomposition product also has been reported in the ^{19}F NMR spectra of $FXeN(SO_2F)_2$ and $Xe[N(SO_2F)_2]_2$ in BrF_5 and SO_2ClF solvents and has a chemical shift of 58.0 ppm in these solvents.[13] The fluorine-on-sulfur resonances of the neutral species $Xe[N(SO_2F)_2]_2$ (SO_2ClF solvent)[11] and $FXeN(SO_2F)_2$ (BrF_5 solvent)[13] have also been reported at 60.2 and 57.6 ppm, respectively, supporting the assignment of the 67.9 ppm peak to $XeN(SO_2F)_2^+$. The ^{19}F NMR spectrum therefore provides convincing evidence for the existence of the $XeN(SO_2F)_2^+$ cation in SbF_5 solution.

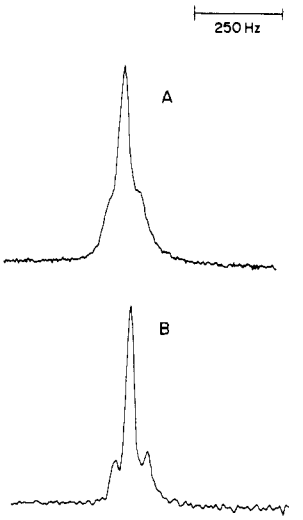

Figure 5. ^{129}Xe NMR spectra (2.3488 T) of the $XeN(SO_2F)_2^+$ cation recorded at 23 °C in SbF_5 solvent: (A) free induction decay transformed by using a Lorentzian fit; (B) free induction decay transformed by using a Gaussian fit.

The ^{15}N NMR spectrum (recorded at 5.8719 T) shows two signals at −212.5 and −243.0 ppm corresponding to the nitrogen environments of the $[N(SO_2F)_2]_2$ decomposition product and the $XeN(SO_2F)_2^+$ cation, respectively. The chemical shift arising from the decomposition product is in good agreement with previously reported values in BrF_5 (−213.1 ppm) and SO_2ClF (−212.3 ppm).[11,13] The ^{15}N chemical shift of the $XeN(SO_2F)_2^+$ cation (Table III) is at slightly higher frequency compared to the neutral compounds $FXeN(SO_2F)_2$ and $Xe[N(SO_2F)_2]_2$ because of the deshielded nature of the electron-poor cation, supporting the existence of the cationic species $XeN(SO_2F)_2^+$ in SbF_5 solution. Interestingly, no ^{15}N–^{129}Xe spin–spin coupling could be observed in the ^{15}N spectrum at 5.8719 T. The absence of a resolved coupling is attributable to relaxation arising from shielding anisotropy effects at high magnetic field strengths (see below).

Further direct evidence for the existence of the $XeN(SO_2F)_2^+$ cation in solution has been obtained with use of ^{129}Xe NMR spectroscopy (Table III). Spectra were obtained at 5.8719 T and consisted of a single resonance at −1945 ppm. The ^{129}Xe chemical shift of $XeN(SO_2F)_2^+$ is at a frequency expectedly higher than those of the neutral compounds $FXeN(SO_2F)_2$ (−1997 ppm, BrF_5 solvent at −58 °C) and $Xe[N(SO_2F)_2]_2$ (−2257 ppm, SO_2ClF solvent at −40 °C).[11,13] The peak obtained at 5.8719 T was Lorentzian in shape with a line width of 139 Hz. No satellite doublet arising from ^{129}Xe–^{15}N spin–spin coupling could be resolved. The line broadening and, consequently, the low resolution of the ^{129}Xe resonance at 5.8719 T is attributed to relaxation dominated by shielding anisotropy (SA) which is field dependent and becomes significant for heavy nuclei. The contribution to the components of the spin–lattice relaxation (T_1) arising from SA is inversely proportional to the square of the external magnetic field B_0 and is given by eq 6, where ω is the resonance frequency,

$$T_1 = \frac{15(1 + \omega^2\tau_c^2)}{\gamma^2 B_0^2(\sigma_\parallel - \sigma_\perp)^2 2\tau_c} \quad (6)$$

γ is the magnetogyric ratio, τ_c is the molecular correlation time, and $\sigma_\parallel$ and $\sigma_\perp$ refer to the shielding along and perpendicular to the symmetry axis, respectively. As B_0 increases, one can clearly see that T_1 decreases, which implies the lifetime of the spin state is correspondingly shortened and the resonance line broadened.

To overcome the line-broadening effects attributed to SA, the same sample was run at room temperature at 2.3488 T. The resulting spectrum (trace A in Figure 5) consisted of one signal at −1946 ppm with shoulders approximately one-third the way up on each side of the Lorentzian curve. To further enhance the

(28) Edwards, A. J.; Jones, G. R.; Sills, R. J. C. *J. Chem. Soc., Chem. Commun.* **1968**, 1527.
(29) Bacon, J.; Dean, P.; Gillespie, R. J. *Can. J. Chem.* **1970**, *48*, 3413.
(30) Schrobilgen, G. J.; Holloway, J. H.; Granger, P.; Brevard, C. *Inorg. Chem.* **1978**, *17*, 980.

Table III. ^{129}Xe and ^{15}N NMR Parameters for $XeN(SO_2F)_2^+$ and Related Xenon(II) Species

species	solvent	temp, °C	$\delta_{^{129}Xe}$[a]	$\delta_{^{15}N}$[b]	$^1J_{^{129}Xe-X}$, Hz	$^1K_{Xe-X}$, 10^{22} N A^{-2} m^{-3}
XeF^+[c]	SbF_5	25	−574		7210	2.307
XeF_2	SO_2ClF	25	−1905		5579	1.785
$XeN(SO_2F)_2^+$	SbF_5	25	−1943	−243.0	91.7	0.272
$Xe[N(SO_2F)_2]_2$[d]	SO_2ClF	−40	−2257	−232.5	259	0.769
$FXeN(SO_2F)_2$[d]	SO_2ClF	−40	−2009	−247.9	307[e]	0.912
					5586[f]	1.787

[a] Referenced with respect to neat $XeOF_4$ at 24 °C. [b] Referenced with respect to neat CH_3NO_2 at 24 °C. [c] Reference 30. [d] Reference 13. [e] $^1J_{^{129}Xe-^{15}N}$. [f] $^1J_{^{129}Xe-^{19}F}$.

resolution, the free induction decay was transformed, from the time to the frequency domain, with use of a Gaussian multiplier rather than the more conventional Lorentzian multiplier. Trace B in Figure 5 depicts the resulting signal, which clearly shows a satellite doublet corresponding to $J_{^{129}Xe-^{15}N}$ = 91.7 Hz. The satellites arising from ^{129}Xe bonded to ^{15}N occur at slightly lower frequency (15.5 Hz) than the singlet arising from ^{129}Xe bonded to ^{14}N, giving the asymmetric appearance to the set of signals. This isotopic shift is 0.56 ppm and represents the small difference in chemical shift between a ^{129}Xe atom bonded to ^{15}N and a ^{129}Xe atom bonded to ^{14}N.

The $^{129}Xe-^{15}N$ coupling in $XeN(SO_2F)_2^+$ of 91.7 Hz represents an apparent decrease from the coupling constants in $FXeN(SO_2F)_2$ and $Xe[N(SO_2F)_2]_2$ of 307 and 259 Hz, respectively.[13] The Fermi contact mechanism is assumed to be dominant, over dipolar and spin–orbital effects, for Xe–N nuclear spin–spin coupling. The mechanism involves direct interaction of the nuclear spin moment with the electron spin moment, which is increased by the probability that the s electrons will be at the nuclei, i.e. bonds with more s character. The Xe–N σp–σsp^2 bonding in the neutral bis compound is modified to Xe–N σsp^3–σsp^2 bonding upon removal of one $N(SO_2F)_2$ ligand to form the cation. One would therefore expect the s character and hence the magnitude of the ^1J coupling to increase from the neutral to the cationic species on the basis of eq 7. The term $|\psi_{ns,A}(0)|^2|\psi_{ns,B}(0)|^2\pi_{A,B}$ describes the probability

$$^1J_{AB} = \frac{16\pi^2}{9h}\left(\frac{g\beta h^2}{2\pi}\right)\gamma_A\gamma_B|\psi_{ns,A}(0)|^2|\psi_{ns,B}(0)|^2\pi_{A,B} \quad (7)$$

of finding an s electron at each of the two nuclei (A and B). An increase in $^1J_{^{129}Xe-^{19}F}$ does occur in the analogous pairs of Xe–F compounds XeF_2, XeF^+ and $FXeN(SO_2F)_2$, XeF^+ as shown in Table III and can be accounted for by using the above argument. To explain the apparent reverse trend in the $^{129}Xe-^{15}N$ couplings, the reduced coupling constants $^1K_{Xe-N}$ and $^1K_{Xe-F}$ were calculated by using eq 8 for $Xe[N(SO_2F)_2]_2$, $FXeN(SO_2F)_2$, $XeN(SO_2F)_2^+$,

$$^1K_{AB} = \frac{4\pi^2}{h\gamma_A\gamma_B}{}^1J_{AB} \quad (8)$$

XeF_2, and XeF^+ and are also listed in Table III. The reduced coupling constant here is the one-bond $^1J_{AB}$ coupling constant with the magnetogyric ratios factored out. The magnitude of the reduced coupling constant is, therefore, a better representation of the electronic environment in a molecule, because it removes the nuclear dependence so one may compare structurally related effects on the spin–spin coupling between different sets of nuclei. In addition to differences in magnitude of magnetogyric ratios, it should be noted that the signs of $\gamma_{^{15}N}$ and $\gamma_{^{129}Xe}$ are both negative and $\gamma_{^{19}F}$ is positive and that the K and J coupling constants obtained from direct measurement of the ^{129}Xe NMR spectrum merely represent absolute values. The differences in reduced coupling constants for $XeN(SO_2F)_2^+/Xe[N(SO_2F)_2]_2$ and XeF^+/XeF_2 were calculated and found to be remarkably similar in magnitude but opposite in sign, i.e., $\mp 0.497 \times 10^{22}$ and $\pm 0.522 \times 10^{22}$ N A^{-2} m^{-3} for Xe–N and Xe–F reduced couplings, respectively. This suggests that the values of $^1K_{Xe-N}$ in the Xe–N compounds are opposite in sign with respect to their one-bond Xe–F counterparts but as a consequence of the negative sign of $\gamma_{^{15}N}$ and the positive sign of $\gamma_{^{19}F}$, $^1J_{^{129}Xe-^{15}N}$, and $^1J_{^{129}Xe-^{19}F}$ have the same sign. On the basis of previously established trends among row 5 spin–spin couplings to ^{19}F,[39] the sign of $^1J_{^{129}Xe-^{19}F}$ is generally taken to be negative. If we bear in mind that $\gamma_{^{129}Xe}$ is negative, the decrease in $^1K_{Xe-N}$ from $[^{15}N]$-$Xe[N(SO_2F)_2]_2$ to $[^{15}N]$-$XeN(SO_2F)_2^+$ can be attributed to an increase from a negative value to a less negative value of $^1K_{Xe-N}$ and would therefore be analogous to the trend in $^1K_{Xe-F}$ observed for the XeF and XeF^+ analogues. This suggests that $^1J_{^{129}Xe-^{15}N}$ and $^1J_{^{129}Xe-^{19}F}$ for both series are negative in sign.

Raman Spectra of $XeN(SO_2F)_2^+AsF_6^-$, $XeN(SO_2F)_2^+Sb_3F_{16}^-$, and $F[XeN(SO_2F)_2]_2^+AsF_6^-$. The Raman spectra (−196 °C) of the cations $XeN(SO_2F)_2^+$ (AsF_6^- and $Sb_3F_{16}^-$ salts) and $F[XeN(SO_2F)_2]_2^+$ (AsF_6^- salt) are illustrated in Figure 6. For the purposes of assigning the Raman bands of $XeN(SO_2F)_2$ moieties, the vibrations associated with the $XeN(SO_2F)_2^+$ cation and its counteranion in each salt were treated separately. From the crystal structure of $XeN(SO_2F)_2^+Sb_3F_{16}^-$, the cation can be assigned to a C_1 point group or to a slightly distorted C_2 point group. In either case, there are 24 vibrational modes ($\Gamma(C_1)$ = 24 A, $\Gamma(C_2)$ = 12 A + 12 B), all of which are both Raman- and infrared-active. Assuming that the $XeN(SO_2F)_2$ group(s) in the AsF_6^- salts possess C_{2v}, C_2, C_s, or C_1 symmetries, all of which give rise to 24 Raman-active bands, it is noteworthy that considerably more than 24 bands attributable to the $XeN(SO_2F)_2$ groups are actually observed for $XeN(SO_2F)_2^+AsF_6^-$, $XeN(SO_2F)_2^+Sb_3F_{16}^-$, and $F[XeN(SO_2F)_2]_2^+AsF_6^-$ (56, 37, and 37 bands, respectively). With use of the present crystallographic findings, a factor-group analysis has been performed for the $XeN(SO_2F)_2^+Sb_3F_{16}^-$ salt using the correlation method.[31] The site symmetry of the $XeN(SO_2F)_2^+$ cation within the primitive unit cell is C_1. The free cation symmetry (C_1 or C_2) has been correlated to the site symmetry of the cation (C_1) which, in turn, has been correlated to the symmetry of the unit cell (C_{2h}) (Table IV (supplementary material)). This correlation predicts that each Raman band of the $XeN(SO_2F)_2^+$ cation will be split into A_g and B_g components (A_u and B_u in the infrared spectrum) under C_{2h} crystal symmetry. Thus, 48 Raman-active bands corresponding to vibrational coupling of the normal modes of the $XeN(SO_2F)_2^+$ cation within the unit cell should result. Depending upon the size of the splitting and spectrometer resolution, only a fraction of these splittings may actually be observable.

The assignments for the Raman spectra of $XeN(SO_2F)_2^+AsF_6^-$, $XeN(SO_2F)_2^+Sb_3F_{16}^-$, and $F[XeN(SO_2F)_2]_2^+AsF_6^-$ (Table V) are based mainly on previous assignments for the related neutral molecules $Xe[N(SO_2F)_2]_2$ and $FXeN(SO_2F)_2$[13] and salts containing the AsF_6^- and $Sb_3F_{16}^-$ anions ($XeF^+AsF_6^-$, $Xe_2F_3^+AsF_6^-$, $ReF_6^+Sb_3F_{16}^-$, and $PF_4^+Sb_3F_{16}^-$).[31-34]

Frequencies can be readily assigned to the SO_2 stretches, the SO_2 bends, the SO_2F torsional modes, and the SF stretching and wagging modes by comparison with the frequencies observed for these vibrations in the neutral compounds $FXeN(SO_2F)_2$ and $Xe[N(SO_2F)_2]_2$ (Table V). In the $XeN(SO_2F)_2^+$ and $F[XeN(SO_2F)_2]_2^+$ cations, nine vibrations may be attributed to the SO_2F group: SO_2 symmetric and asymmetric stretches, an SO_2 bend,

(31) Fateley, W. G.; Dollish, F. R.; McDevitt, N. T.; Bentley, F. F. "Infrared and Raman Selection Rules for Molecular and Lattice Vibrations: The Correlation Method"; Wiley-Interscience: New York, 1972.
(32) Gillespie, R. J.; Landa, B. *Inorg. Chem.* **1973**, *12*, 1383.
(33) Schrobilgen, G. J.; Holloway, J. H.; Russell, D. R. *J. Chem. Soc., Dalton Trans.* **1984**, 1411.
(34) Passmore, J.; Chen, G. S. H. *J. Chem. Soc., Dalton Trans.* **1979**, 1251.

Table V. Raman Spectra of $XeN(SO_2F)_2^+AsF_6^-$, $XeN(SO_2F)_2^+Sb_3F_{16}^-$,[a] $F[XeN(SO_2F)_2]_2^+AsF_6^-$, and $FXeN(SO_2F)_2$ with Their Tentative Assignments

freq, cm^{-1}				
$XeN(SO_2F)_2^+AsF_6^-$	$XeN(SO_2F)_2^+Sb_3F_{16}^-$	$F[XeN(SO_2F)_2]_2^+AsF_6^-$	$FXeN(SO_2F)_2$[b]	approx descripn
1492 (9) 1489 (19) 1483 (2)	1501 (20) 1496 (13)	1490 (62) 1473 (3)	1451 (14) 1449 (24)	SO_2 asym str, i
1475 (4) 1470 (5) 1460 (1) 1455 (1)	1482 (4) 1477 (8) 1467 (1)	1442 (1) 1458 (7)	1439 (2) 1425 (19)	SO_2 asym str, o
1233 (39) 1230 sh	1248 (23) 1239 (44)	1237 (14) 1228 (32)	1209 (10) 1206 sh	SO_2 sym str, i and o
914 (3) 908 (3) 900 (3) 889 (18) 885 (20) 879 (21) 875 (17)	890 (19) 884 (23)	904 (100)	888 (33) 881 (11)	SNS asym str
844 (16) 842 sh	838 (21)	829 (28)	842 (4) 836 (13)	SF str, i and o
830 (26)	826 (17) 812 (6)	823 (22)	825 (17) 797 (23)	SNS sym str
633 (12)	655 (100) 630 (20) 602 (8)	644 (54)	656 (41)	SO_2 bend, o
554 (1) 547 (1)	556 (11) 552 sh 542 (20)	557 (3) 553 (4)	559 (8) 551 (7)	SO_2 ⊥ rock, i
527 (2) 511 (4) 509 (5)	523 (3) 508 (5)	533 (4) 514 (4) 510 (2)	514 (6) 506 (100)	SO_2 bend, i Xe–F str
478 (12) 471 (9)	483 (30) 475 sh	484 (36) 475 (14)	478 (17)	SO_2 ∥ rock, i and o
452 (1)			469 (17)	SF ∥ wag
		423 (2)	422 (4) 417 (1)	Xe–^{14}N str Xe–^{15}N str
413 (4) 387 (4)	408 (3) 386 (5)	406 (3) 385 (3)	340 (52)	SNS bends
317 (35)	314 (26)	335 (14) 330 (12)		Xe---F str
296 (10)	294 (19)	303 (5)	312 (18)	SF ⊥ wag, i and o
287 (57)	290 (23)	288 (8)	286 (22)	SO_2F torsion, i and o
264 (3) 259 (2) 251 (10) 241 (100) 226 (3)	267 (12) 256 (37) 248 (84) 240 (16)	264 (49) 260 (18) 247 (6) 240 (10) 231 (21) 224 (35) 208 (24)		XeNS bends (cations)
			220 (113) 215 (87)	XeNS bends (neutral $FXeN(SO_2F)_2$ compd)
			186 (13) 180 (7) 141 (43) 119 (28) 116 (27) 111 (31) 96 (22)	F–Xe–N bends
163 (18) 160 (14) 154 (16) 151 (9) 125 (6) 114 (3) 111 (4) 104 (9)	163 (9) 155 sh 150 (23) 114 (7)	166 (5) 105 (3)		F---Xe–N bends

Table V (Continued)

freq, cm^{-1}				
$XeN(SO_2F)_2^+AsF_6^-$	$XeN(SO_2F)_2^+Sb_3F_{16}^-$	$F[XeN(SO_2F)_2]_2^+AsF_6^-$	$FXeN(SO_2F)_2$[b]	approx descripn
721 (9)				$\nu_8(e)$, $(F\cdots AsF_5)^-$
717 (7)				
674 (48)				$\nu_1(a_1)$, $(F\cdots AsF_5)^-$
598 (10)				$\nu_5(b_1)$, $(F\cdots AsF_5)^-$
589 (1)				
578 (1)				
567 (4)				
396 (1)				$\nu_{10}(e)$, $(F\cdots AsF_5)^-$
382 (5)				$\nu_9(e)$, $(F\cdots AsF_5)^-$
376 (2)				
	721 (3)			Sb–F str
	717 (9)			
	709 (39)			
	689 (25)			
	683 sh			
	667 (20)			
		682 (10)		$\nu_1(a_{1g})$, AsF_6^-
		680 (18)		
		583 (2)		$\nu_2(e_g)$, AsF_6^-
		574 (2)		
		570 (2)		
		379 (3)		$\nu_5(t_{2g})$, AsF_6^-
		374 (3)		
	277 (10)			Sb–F bends
	220 (6)			
	216 (7)			
	200 (1)			
75 (15)	75 (4)	91 (39)	87 (6)	lattice modes
62 (26)		75 (4)	60 sh	
57 (10)			56 (16)	
54 (9)			55 sh	
47 (29)			50 (111)	
			46 (57)	

[a] The Raman spectrum of $XeN(SO_2F)_2^+Sb_3F_{16}^-$ was recorded in a glass tube at −196 °C; all other compound spectra were recorded in FEP sample tubes at −196 °C. Values in parentheses denote intensities. Abbreviations: str, stretching vibration(s); sym and asym, symmetric and asymmetric vibration(s); i, in-phase vibration(s); o, out-of-phase vibration(s) (attributed to coupling of SO_2F group modes in the same $N(SO_2F)_2$ group); ∥, parallel to SNS plane; ⊥, perpendicular to SNS plane; sh, shoulder. [b] Reference 13.

two SO_2 rocks, an SF stretch, two SF wags, and an SO_2F torsion (the SO_2 rocking and SF wagging vibrations can occur parallel or perpendicular to the SNS plane). Each of these generally gives rise to two lines in the spectrum (with coupling between molecules in the unit cell being ignored). These are regarded as arising from coupling between the two SO_2F groups, and they are described as in-phase and out-of-phase motions of these groups. Three vibrations may be assigned to the SNS bridging group: a symmetric stretch, an asymmetric stretch, and a bend. The ^{129}Xe–^{14}N stretch in the $XeN(SO_2F)_2^+$ cation (630, 633 cm^{-1}) is at higher frequency than in the neutral compound (422 cm^{-1}), indicating a stronger, shorter Xe–N bond in the cation. It is noteworthy that the lower frequency ^{129}Xe–^{15}N stretch (598, 602 cm^{-1}) is also observed for the $XeN(SO_2F)_2^+$ cation, which is 30% nitrogen-15 enriched. The bridging Xe···F stretch is also observed for the $F[XeN(SO_2F)_2]_2^+$ cation at a much lower frequency (335 cm^{-1}) than the stretch for the correspondingly more covalent Xe–F bond in $FXeN(SO_2F)_2$ (506 cm^{-1}). However, this bridging Xe···F stretching frequency is comparable to other previously reported Xe···F stretching modes (339 and 337 cm^{-1} for $XeF^+AsF_6^-$ and $XeF^+SbF_6^-$, respectively).[31] Both the Xe–F bond length and ionic character of an FXeY system are reflected in the observed frequencies of the Xe···F and Xe–F stretches, with a low-frequency stretch (339 cm^{-1}, $FXe\cdots FAsF_5$) indicating a bridge bond interaction and a higher frequency (609 cm^{-1}, $F\text{–}XeFAsF_5$)[31] indicating a much more covalent terminal Xe–F bond. The F···Xe–N group is expected to contribute two types of bending vibrations: F···Xe–N and Xe–N–S bends parallel and perpendicular to the SNS plane. Bends occurring parallel to the SNS plane are expected to occur at higher frequencies than their perpendicular counterparts. The XeNS bends will occur at lower frequencies than the SNS bends, because the Xe–N moiety is not a part of the π-bonding system that is involved with nitrogen and sulfur and because of the mass effect of xenon. Finally, the remaining lines below 125 cm^{-1} are attributed to lattice modes.

Experimental Section

Apparatus and Materials. The air- and moisture-sensitive natures of the precursors and products required that all manipulations be carried out under anhydrous conditions on a vacuum line or in a nitrogen-filled drybox (Vacuum Atmospheres Model DLX). Air-sensitive substances of low volatility, i.e., $[^{15}N]\text{-}HN(SO_2F)_2$, $[^{15}N]\text{-}FXeN(SO_2F)_2$, $[^{15}N]\text{-}F[XeN(SO_2F)_2]_2^+AsF_6^-$ and SbF_5, were transferred in a drybox. The vacuum line used to transfer more volatile substances was constructed from 316 stainless steel, nickel, Teflon, Kel-F, and FEP.

The preparations of AsF_5[34] and $[^{15}N]\text{-}FXeN(SO_2F)_2$[11] have been described elsewhere. Antimony pentafluoride (Ozark Mahoning) was purified by static vacuum distillation at room temperature and condensed at −78 °C with use of an all-glass apparatus.

$[^{15}N]\text{-}XeN(SO_2F)_2^+AsF_6^-$ and $[^{15}N]\text{-}F[XeN(SO_2F)_2]_2^+AsF_6^-$. Nitrogen-15-enriched (30%) $XeN(SO_2F)_2^+AsF_6^-$ and $F[XeN(SO_2F)_2]_2^+AsF_6^-$ were prepared according to eq 1 and 2. In a typical preparation, 2.5 g of 30% ^{15}N-enriched $FXeN(SO_2F)_2$ was placed in an FEP reaction vessel equipped with a Kel-F valve. A 10-fold molar excess of AsF_5 was condensed onto the sample at −78 °C (vapor pressure 225 mmHg) and maintained at this temperature for 8 h. The partially reacted sample was then slowly warmed to room temperature, and the excess of AsF_5 was allowed to expand into the vacuum manifold and adjusted to a total pressure of 1600 torr at room temperature. The sample pressure was periodically readjusted to 1600 torr as the reaction proceeded over the next $^1/_2$ h. The AsF_5 was recondensed, wetting the entire sample, and warmed as above. The condensing–warming cycles were repeated a total of three times before the sample was allowed to stand at −78 °C under

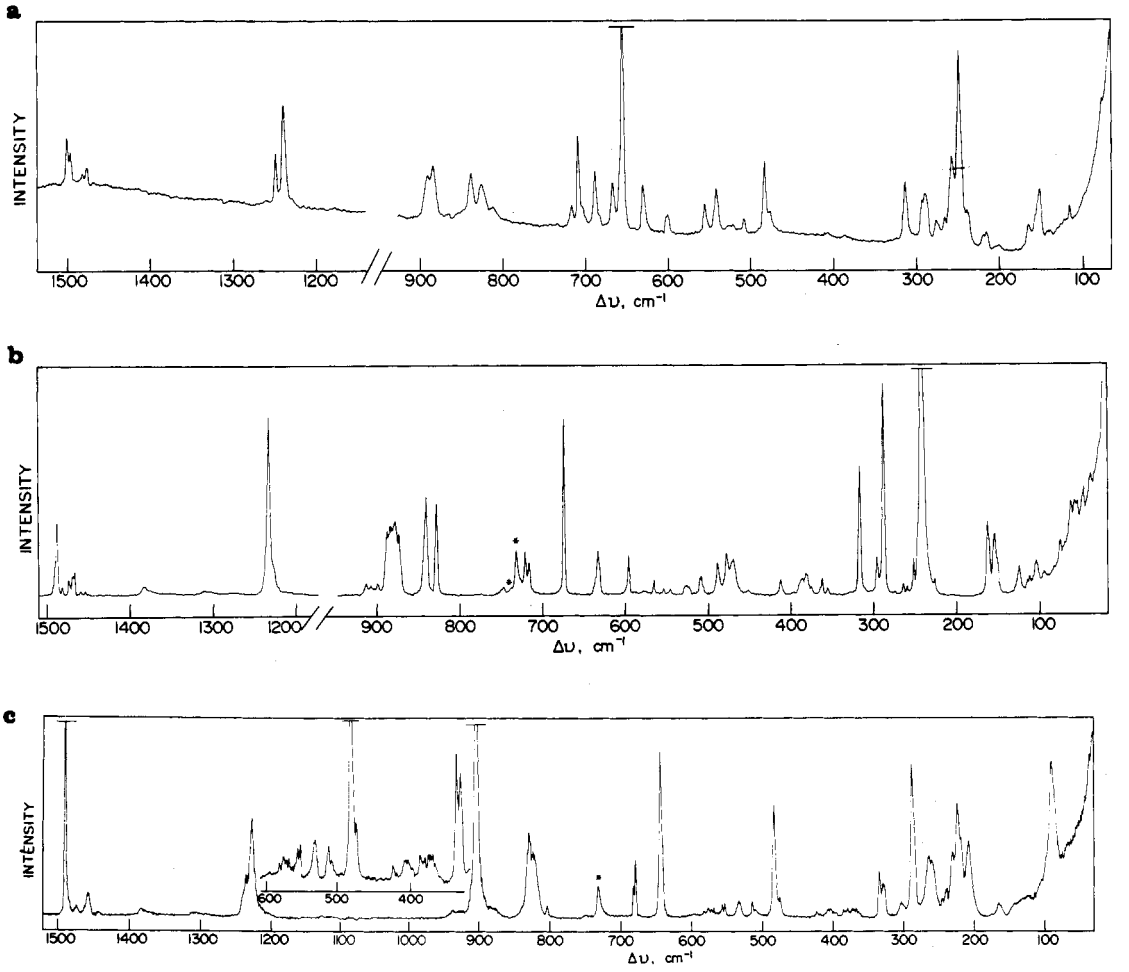

Figure 6. Raman spectra recorded at −196 °C with 514.5-nm excitation (asterisks denote FEP sample tube lines): (a) $XeN(SO_2F)_2^+Sb_3F_{16}^-$; (b) $XeN(SO_2F)_2^+AsF_6^-$; (c) $F[XeN(SO_2F)_2]_2^+AsF_6^-$.

approximately 1 cm of liquid AsF_5 for an additional 8-h period. The AsF_5 was then slowly removed under vacuum at −78 °C until a dry, light yellow microcrystalline powder was left. The light yellow compound, $XeN(SO_2F)_2^+AsF_6^-$, was found to be thermally unstable at room temperature and was stored at −78 °C under a positive pressure of dry N_2 gas until used. The corresponding bis cation was formed by warming $XeN(SO_2F)_2^+AsF_6^-$ to room temperature and pumping off the excess AsF_5 for ca. $1^1/_2$ h (see eq 2).

$XeN(SO_2F)_2^+Sb_3F_{16}^-$. The ^{15}N-enriched title compound was prepared according to eq 9. A quantity of $[^{15}N]$-$F[XeN(SO_2F)_2]_2^+AsF_6^-$ (ca. 0.3

$$F[XeN(SO_2F)_2]_2^+AsF_6^- + 3SbF_5 \xrightarrow{SbF_5} 2XeN(SO_2F)_2^+Sb_3F_{16}^- + AsF_5 \quad (9)$$

g) was transferred to a 10 mm o.d. glass reaction tube in a drybox. Excess SbF_5 was then carefully syringed into the top portion of the tube. The high viscosity of liquid SbF_5 ensured that it would not flow quickly and come into direct contact with $F[XeN(SO_2F)_2]_2^+AsF_6^-$ immediately. The heat generated from the highly exothermic reaction of SbF_5 with $F[XeN(SO_2F)_2]_2^+AsF_6^-$ is sufficient to cause rapid decomposition of the product if the temperature of the reaction mixture is not carefully controlled. A Teflon valve was attached to the Pyrex reaction vessel by means of Teflon compression fittings prior to bringing the vessel out of the drybox. The SbF_5 was then allowed to come slowly in contact with $F[XeN(SO_2F)_2]_2^+AsF_6^-$, while the reaction temperature was moderated by repeated cooling of the vessel in an ice–water bath. The mixture was subsequently agitated at room temperature for approximately $^1/_2$ h to ensure complete reaction, and the evolved AsF_5 was pumped off and the sample heat-sealed under vacuum. The product slowly crystallized in the SbF_5 solution at room temperature after standing for ca. 5 h followed by decanting the residual SbF_5 solution into the top portion of the tube. The tube was then transferred to a drybox and cut in half. The tube portion containing the SbF_5-coated crystals was placed in a dry FEP vessel and evacuated at room temperature to remove residual SbF_5. The remaining free-flowing yellow crystals, which decompose slowly at room temperature, were stored at 0 °C under a positive pressure of dry N_2 gas until used.

X-ray Crystallography. Crystals of $XeN(SO_2F)_2^+Sb_3F_{16}^-$, prepared from SbF_5 solution as previously described, were transferred in a drybox into quartz capillary tubes and temporarily sealed off with dry Kel-F wax. The capillary tubes were taken out of the drybox and permanently sealed with a microtorch. Owing to their thermal instability, the crystals were stored at −78 °C until they could be examined.

Crystal data: $XeNS_2O_4F_{18}Sb_3$, fw = 980.65, monoclinic, space group $P2_1/c$, a = 10.320 (2) Å, b = 10.642 (2) Å, c = 18.167 (3) Å, β = 108.94 (1)°, V = 1887.2 (4) Å^3, Z = 4. Mo Kα radiation (λ = 0.710 69 Å, μ(Mo K$\bar{\alpha}$) = 56.1 cm^{-1}) was used.

X-ray Intensity Measurements. A light yellow crystal of the title compound, sealed in a quartz capillary, was approximately plate shaped with the dimensions 0.13, 0.06, and 0.22 mm. The crystals decomposed within a few hours at room temperature, so all X-ray work was performed at −64 ± 1 °C with a Nicolet $P2_1$ diffractometer with an LT-1 low-temperature device.

Precession photographs of zero and first layers suggested the crystal was monoclinic and possessed the space group $P2_1/c$, based on the systematic absences.

The crystal was transferred to a Nicolet $P2_1$ diffractometer and was mounted roughly along b. Accurate parameters were obtained from a least-squares fit of χ, ϕ, and 2θ for 15 medium-angle ($18° < 2\theta < 29°$) reflections. With Z = 4, ρ(calcd) was 3.45 g/cm^{-3} and the linear absorption coefficient was 63.0 cm^{-1}. Intensities were measured for the quadrant, $h,k,\pm l$ up to 2θ = 45°, with use of the $P2_1$ diffractometer and graphite-monochromated Mo Kα radiation. Data were collected with a coupled θ(crystal)–2θ(counter) scan 1° on either side of the peak with scan rates varying from 5 to 24° min^{-1}, which were dependent on the intensity of a prescan. Stationary-background counts with a time equal to one-fourth of the scan time for each reflection were made at each end of the scan range. Two standard reflections, which were monitored after every 48 reflections were collected, showed no significant variation in intensity over the period of the data collection. The counting esd's of the standard peaks were 1.3% and 1.4%, and an analysis of the standard counts showed an overall esd of 1.5% with no systematic variation with time. A total of 2475 reflections (including standards) in quadrants with $2\theta \leq 45°$ was collected.

Table VI. Atomic Positional Coordinates and Temperature Factors

atom	$10^{-4}x$	$10^{-4}y$	$10^{-4}z$	$10^{-3}U_{eq}$, Å^2
Xe	−3372 (1)	−739 (1)	3812 (1)	22.7
N	−4360 (10)	−2390 (10)	3509 (7)	25.9
S(1)	−3424 (4)	−3676 (4)	3446 (2)	27.4
S(2)	−6025 (4)	−2451 (5)	3432 (3)	55.0
O(11)	−4250 (10)	−4450 (10)	2866 (6)	44.5
O(12)	−2140 (10)	−3215 (9)	3477 (5)	33.2
F(1)	−3278 (8)	−4282 (8)	4225 (5)	38.1
O(21)	−6690 (10)	−2340 (20)	2645 (8)	132.9
O(22)	−6250 (10)	−3560 (10)	3730 (10)	69.2
F(2)	−6260 (10)	−1370 (10)	3810 (10)	193.2
F(11)	−2123 (8)	1244 (8)	4216 (5)	37.7
Sb(1)	−871 (1)	2592 (1)	4592 (1)	23.6
F(12)	490 (9)	3777 (9)	4800 (5)	50.3
F(13)	−2032 (9)	3589 (9)	3832 (5)	43.7
F(14)	325 (8)	1408 (9)	5171 (5)	40.5
F(15)	−1594 (9)	3009 (9)	5353 (5)	51.2
F(21)	−136 (8)	2023 (8)	3717 (4)	36.0
Sb(2)	334 (1)	759 (1)	3027 (1)	29.1
F(22)	−478 (9)	1853 (9)	2251 (5)	48.4
F(23)	1303 (9)	−6 (9)	3946 (5)	51.0
F(24)	910 (10)	−311 (8)	2393 (5)	63.8
F(25)	−1257 (9)	−70 (10)	2987 (5)	66.1
F(32)	1981 (8)	1779 (9)	3198 (5)	43.2
Sb(3)	3610 (1)	2882 (1)	3874 (1)	24.7
F(31)	2260 (10)	4074 (9)	3749 (4)	57.7
F(33)	3160 (10)	2214 (9)	4705 (4)	49.1
F(34)	4624 (9)	1462 (9)	3866 (6)	49.2
F(35)	5078 (9)	3810 (10)	4483 (5)	54.4
F(36)	3802 (8)	3343 (8)	2929 (5)	41.8

Lorentz and polarization corrections were applied to all data, but no correction was made for absorption. This will introduce a maximum error in F_o of 23%. After equivalent reflections (R_{merge} = 0.024) were averaged and reflections that were systematically absent or had F_{obsd} = 0.0 were excluded, a total of 2376 reflections was obtained and used in the subsequent refinements.

Structure Solution. The structure was solved by the use of the Patterson function to locate the xenon and antimony atoms. Subsequent cycles of least-squares and Fourier calculations located all the remaining atoms in the structure. Full-matrix least-squares refinement with all atoms having anisotropic thermal parameters and including a correction for isotropic extinction minimized the function $\sum w(|F_o| - |F_c|)^2$ converged to the agreement indices R_1 = 0.061 and R_2 = 0.043 for 2376 observed ($F > 0.0$) reflections. In the final cycle of refinement no parameter shifted by more than 1% of its standard error and weights were given by $w^{-1} = \sigma(F)^2 + 0.0003F^2$. The final difference Fourier contained a maximum residual peak of +1.5 e Å^{-3} and a minimum trough of −1.5 e Å^{-3}, close to the xenon atom. The final value of the extinction parameter g as defined by the XRAY system[35] was 1.6×10^{-4}. Scattering factors and anomalous dispersion corrections were taken from ref 36.

All calculations were performed on a Cyber computer with the use of the series of programs in the XRAY 76[37] and SHELX[38] systems, as well as some local programs. The final atomic positions are given in Table VI and interatomic distances, angles, and some significant contact distances in Table I. Final structure factor tables and a listing of anisotropic thermal parameters have been deposited as supplementary material.

Nuclear Magnetic Resonance Spectroscopy. All spectra were recorded unlocked (field drift <0.1 Hz h^{-1}) at 24 °C on commercial pulse spectrometers equipped with superconducting magnets. The high-field (5.8719-T) ^{19}F, ^{129}Xe, and ^{15}N spectra were obtained on a Bruker WM-250 spectrometer. The low-field (2.3488-T) ^{129}Xe spectra were obtained on a Bruker WP-100 SY/SC spectrometer at 27.84 MHz.

The 5.8719-T ^{19}F and ^{129}Xe spectra were obtained on the same 10-mm probe (broad-banded over the frequency range 23–103 MHz) tuned to 69.50 MHz for ^{129}Xe. Fluorine-19 spectra were obtained with use of the proton decoupler coils retuned to 235.35 MHz as the observe coils. The ^{15}N spectra were obtained at 5.8719 T on a 15-mm probe (broad-banded over the frequency range 10–38 MHz) tuned to 25.33 MHz. The 5.8719-T ^{19}F, ^{129}Xe, and ^{15}N spectra were obtained in 900, 2600, and 1400 scans at spectral width settings of 100 (6.1 Hz/data point, 0.164-s acquisition time), 20 (2.1 Hz/data point, 0.819-s acquisition time), and 10 kHz (1.2 Hz/data point, 0.819-s acquisition time), respectively. The ^{129}Xe spectra recorded at 2.3488 T were recorded (30000 scans) with use of a spectral width of 20 kHz (2.4 Hz/data point, 0.205-s acquisition time). The 5.8719-T ^{129}Xe and ^{19}F free induction decays were accumulated in 32K memories while the ^{15}N and 2.3488-T ^{129}Xe free induction decays were accumulated in 16K memories. The low-field ^{129}Xe spectra were further enhanced by transforming the free induction decays from a time to a frequency domain with use of a Gaussian fit rather than the conventional Lorentzian fit. Pulse widths corresponding to bulk magnetization tip angles, θ, of ~90° were 2 (^{19}F), 22 (^{129}Xe, 5.8719 T), and 20 μs (^{129}Xe, 2.3488 T) and for ^{15}N ($\theta \approx 30°$) was 115 μs. With the exception of ^{15}N, no relaxation delay was applied. For ^{15}N, the delay was 30 s. Line-broadening parameters used in exponential multiplication of the free induction decays were set equal to their respective data point resolutions. All spectra were obtained with precision thin-walled glass NMR tubes (Wilmad) of 10 mm o.d. (^{19}F and ^{129}Xe) and 15 mm o.d. (^{15}N).

The respective nuclei were referenced with respect to neat samples of $CFCl_3$ (^{19}F), $XeOF_4$ (^{129}Xe), and CH_3NO_2 (^{15}N) at 24 °C. The chemical shift convention used is a positive sign signifies a chemical shift to high frequency of the reference compound.

Laser Raman Spectroscopy. A Coherent Inova 90-5 argon ion laser, giving up to 5 W at 514.5 nm, was used to excite the Raman spectra. The spectrometer was a Spex Industries Model 14018 double monochromator equipped with 1800 grooves mm^{-1} holographic gratings. An RCA C 31034 phototube detector in conjunction with a pulse count system consisting of pulse amplifier, analyzer, and rate meter (Hamner NA-11, NC-11 and N-708 A, respectively) and a Texas Instruments Model FSOZWBA strip-chart recorder were used to record the spectra. The spectrometer was periodically calibrated by recording the discharge lines from an argon lamp over the spectral range of interest; the Raman shifts quoted are estimated to be accurate to ±1 cm^{-1}. Slit widths depended on the scattering efficiency of the sample, laser power, etc., with 1.0 cm^{-1} being typical.

Glass NMR (5 mm o.d.) and FEP (6 mm o.d.) sample tubes were mounted vertically. The angle between the incident laser beam and the sample tube was 45°, and Raman scattered radiation was observed at 45° to the laser beam (90° to the sample tube axis).

Low-temperature spectra were recorded at −196 °C by mounting the sample vertically in an unsilvered Pyrex glass Dewar filled with ice-free liquid nitrogen.

Acknowledgment. We wish to thank Dr. J. F. Sawyer, Department of Chemistry, University of Toronto, for useful discussions, Dr. C. A. Rodger, Bruker Spectrospin Canada, Milton, Ontario, Canada, for obtaining the low-field ^{129}Xe NMR spectra reported in this work, and the Natural Sciences and Engineering Research Council of Canada for financial support.

Registry No. $XeN(SO_2F)_2^+AsF_6^-$, 68220-74-6; $F[XeN(SO_2F)_2]_2^+AsF_6^-$, 85883-05-2; $XeN(SO_2F)_2^+Sb_3F_{16}^-$, 99665-06-2; ^{129}Xe, 13965-99-6; ^{15}N, 14390-96-6.

Supplementary Material Available: Listings of anisotropic thermal parameters and observed and calculated structure factors, Figures 2–4, showing a stereoscopic view of the unit cell, the calculated minimum interatomic distance between the SO_2F groups of the $XeN(SO_2F)_2^+$ cation, and the staggered conformation of the SO_2F groups, and Table IV, a correlation diagram for the vibrational modes of the $XeN(SO_2F)_2^+$ cation (17 pages). Ordering information is given on any current masthead page.

(35) Keller, N.; Schrobilgen, G. J. *Inorg. Chem.* **1981**, *20*, 2118.
(36) Cromer, D. T.; Waber, J. T. "International Tables for X-ray Crystallography"; Ibers, J. A., Hamilton, W. C., Eds.; Kynoch Press: Birmingham, England, 1974; Vol. IV, Tables 2.2B and 2.3.1, pp 99–101, 149–150.
(37) "XRAY 76 System of Crystallographic Programs", Technical Report TR-446; Computer Science Center, University of Maryland: College Park, MD, 1976.
(38) Sheldrick, G. M. "SHELX Program for Crystal Structure Determination"; University of Cambridge: Cambridge, England, 1976.
(39) Gillespie, R. J.; Schrobilgen, G. J. *Inorg. Chem.* **1974**, *13*, 1230.